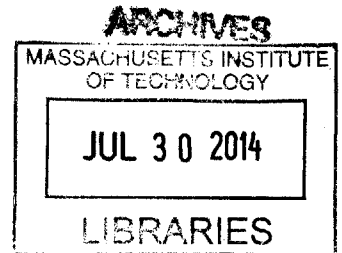


Experimental Design to Determine the Effect of Temperature and Mach Number on Entropy Noise

by **Mariah I. Hake**

Submitted to the Department of Mechanical Engineering
in partial fulfillment of the requirements for the degree of
Bachelor of Science in Engineering as recommended by the
Department of Mechanical Engineering at the



MASSACHUSETTS INSTITUTE OF TECHNOLOGY
June 2014

©2014 Mariah I. Hake. All rights reserved.

The author hereby grants to MIT permission to reproduce
and to distribute publicly paper and electronic
copies of this thesis document in whole or in part
in any medium now known or hereafter created.

Signature redacted

Signature of Author: _____

Department of Mechanical Engineering
April 1, 2014

Certified by: _____

Signature redacted

Kripa K. Varanasi
Associate Professor of Mechanical Engineering
Thesis Supervisor

Accepted by: _____

Signature redacted

Annette P. Hosoi
Associate Professor of Mechanical Engineering
Undergraduate Officer

Experimental Design to Determine the Effect of Temperature and Mach Number on Entropy Noise

by Mariah I. Hake

Submitted to the Department of Mechanical Engineering
on May 9, 2014 in Partial Fulfillment of the
Requirements for the Degree of Bachelor of Science in
Engineering as recommended by the Department of Mechanical Engineering

ABSTRACT

The Osney Laboratory sought to create an entropy noise test rig that could determine the relationship between entropy noise and the flow parameters of temperature change and nozzle Mach number. The apparatus simulates entropy noise in an aero engine. In the test rig, compressed air enters an anechoic labyrinth, flows through a settling chamber that straightens airflow, and then goes to the entropy wave generator. The entropy wave generator forms entropy waves through electric heating. Entropy waves are then accelerated in a convergent-divergent nozzle to produce entropy noise. Microphones at the end of the rig detect entropy noise readings as acoustic sound. Air exits through an anechoic termination. The test rig allows for easy changes in temperature and Mach number so variation in entropy noise with different input values can be tested. Project stages include literature compilation, 3D computer-aided design, part revision, material specification, and finally supervision of manufacture.

Thesis Supervisor: Kripa K. Varanasi
Title: Associate Professor of Mechanical Engineering

ACKNOWLEDGMENTS

For providing knowledge, aid, resources, and mentorship, special thanks to:

Dr. Kripa Varanasi

Supervision and guidance.

Dr. Peter Ireland & Dr. Kam Chana

Oversight in test rig development and contribution of subject knowledge.

Osney Lab Technicians, Gerald Walker, Trevor Godfrey, & Paul Cox

Work toward build and assembly.

Craig Mead

Advice and liaising with Rolls Royce.

Eduard Ron and the Southwell Graduate office at the University of Oxford

Adopting the test rig and continuing forward with experimentation.

TABLE OF CONTENTS

TITLE PAGE	1
ABSTRACT	3
ACKNOWLEDGEMENTS	4
TABLE OF CONTENTS	5
1. INTRODCUTION	6
2. BACKGROUND	7
2.1 Entropy Noise	7
2.2 Experimental Predecessor	9
2.3 Input Parameters	12
3. EXPERIMENTAL DESIGN	13
3.1 Test Rig Apparatus	13
3.2 Anechoic Labyrinth	14
3.3 Settling Chamber	18
3.4 Entropy Wave Generator	19
3.5 Convergent-Divergent Nozzle	27
3.6 Microphones	30
3.7 Anechoic Termination	32
4. METHOD	35
5. CONCLUSIONS	36
REFERENCES	37

1. INTRODUCTION

Aircrafts create sound as they operate. This noise is disturbing to any community within earshot because it can cause annoyance and unwanted health effects. Therefore, aircrafts in the United States are held to strict sound pollution regulations by the EPA according to the Noise Control Act of 1972, which sets noise emission standards for each phase of flight (epa.gov). European countries also have similar noise regulation standards. Consequently, jet manufacturers are continuously searching for new ways to reduce jet noise emissions. Much work has already been done to reduce jet noise generated from the airframe, fans, and exhaust exits. More research emphasis must be placed on aero engine redesign in order to obtain further reductions in noise pollution (Bake 2008). Most typically, the types of engines used in jets are internal combustion engines, which are responsible for generating two kinds of noise: combustion noise and entropy noise.

Entropy noise, rather than combustion noise, is the topic of interest for this project for two reasons. (1) Entropy noise is the dominant source of engine sound during takeoff and landing, when the plane is closest to the ground and the biggest threat for causing disruption through sound pollution (Leyko 2008). (2) Entropy noise is not yet as well understood because it has been studied mostly theoretically and has limited experimental research or data.

The mission at the University of Oxford's Osney Thermo-Fluids Laboratory therefore was to create an entropy noise test rig that could determine the relationship between entropy noise and varying parameters. Through this research, we aimed to have the capacity to learn how adjusting temperature and mass flow could reduce total noise emission from aero engines. Noise research is also being performed by academic staff in the Engineering Science Department at the Oxford Turbine Research Facility. The research will use the turbine test facility to investigate the effect of a non-uniform inlet temperature distribution on entropy noise generation. (eng.ox.ac.uk)

Entropy noise contributes to sound emission from aero engines. Determining how various factors influence entropy noise will enable future engine designs to incorporate this information to reduce sound pollution.

2. BACKGROUND

2.1 Entropy Noise

The components of a jet internal combustion engine are depicted in Figure 1. Air enters the engine through its inlet. Then the compressor increases air pressure and temperature through a series of rapidly rotating blades. The combustor heats the air further until it reaches around 1500 degrees Celsius (rolls-royce.com). In jet combustion chambers, pressure is intended to stay constant as fluid temperature rises. Then the turbine extracts some of the combustor's output energy to power the compressor. Finally, the heated, high velocity air escapes through the engine exhaust nozzle, propelling the jet forward. (cs.stanford.edu)

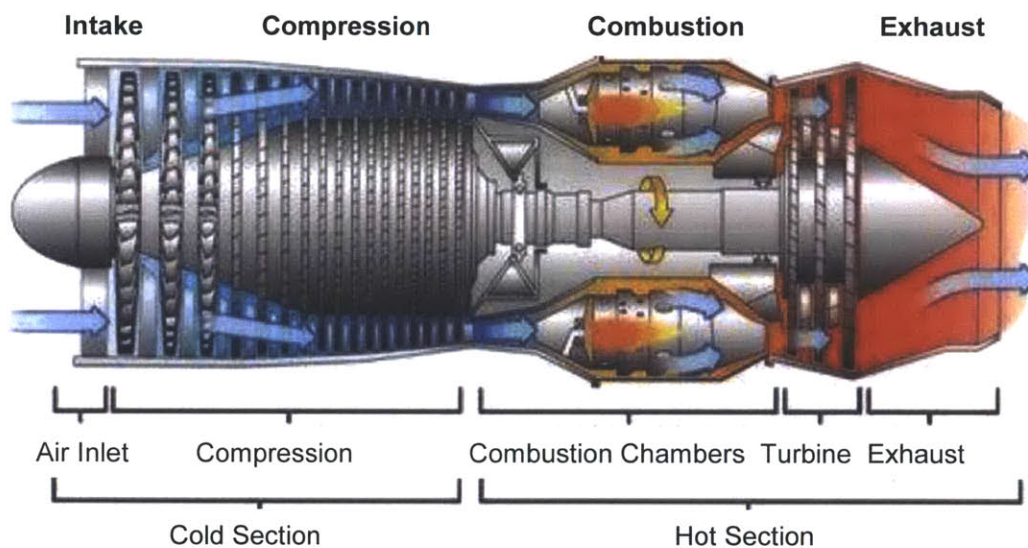


Figure 1: A jet engine has five main components: the air inlet valve, compressor, combustor, turbine, and exhaust nozzle. These components work together to power jet motion. Combustion noise and entropy noise are both generated in the hot section of the engine (shown in orange and red), which is made up of the combustion and exhaust processes. (engg-learning)

As jets operate, internal combustion engines generate combustion noise and entropy noise, also known as direct and indirect noise, respectively. Combustion noise results from flame turbulence in the combustion chamber. Following the ideal gas law, this stochastic heat release produces pressure waves manifested as acoustic sound. This sound gets distorted and reflected in the turbine, exiting louder through the exhaust. (Schwarz 2009)

Like combustion noise, entropy noise is also caused by heat release fluctuations in the combustor. However, entropy noise differs from combustion noise in how the sound is developed within the system. For combustion noise, heat release directly produces acoustic perturbations via pressure waves in the combustor. However, for entropy noise, the unsteady heat release results in an uneven spread of temperature in the fluid, which leads to non-uniform distributions of entropy, called entropy waves. Hot spots, cold spots, and imperfect mixing are all

sources of entropy waves. Entropy noise occurs when these entropy waves convect out of the combustor through the turbine, where they interact with accelerated mean flow and form more pressure waves. Figure 2 illustrates core engine sound formation. (Leyko 2008)

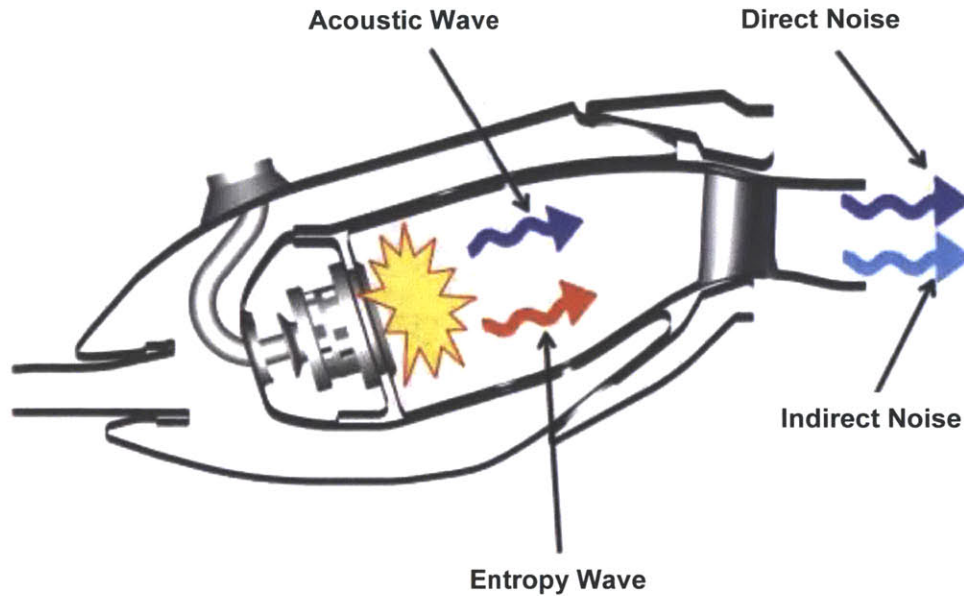


Figure 2: Acoustic waves are formed from flame turbulence in the combustor. This causes direct combustion noise. Entropy waves are also formed in the combustor. When entropy waves accelerate in the turbine section through pressure gradients, this causes indirect entropy noise. (García-Rama 2012)

The Osney Thermo-Fluids laboratory required a test rig that could create and detect entropy noise with various adjustable parameters in order to conduct future experiments related to entropy noise. Obtaining data would foster a better understand of how entropy noise levels shift with different inputs. This research would eventually be applied to new internal combustion engine designs in order to work toward decreasing entropy noise and aggregate sound pollution coming from jets.

2.2 Experimental Predecessor

The German Aerospace Center Institute of Propulsion Technology (DLR), Europe's leading aircraft research institution, has conducted experiments for the same purpose of characterizing entropy noise. They published credible results (see Figure 3) describing the relationship between entropy noise and variables of temperature change and nozzle Mach number.

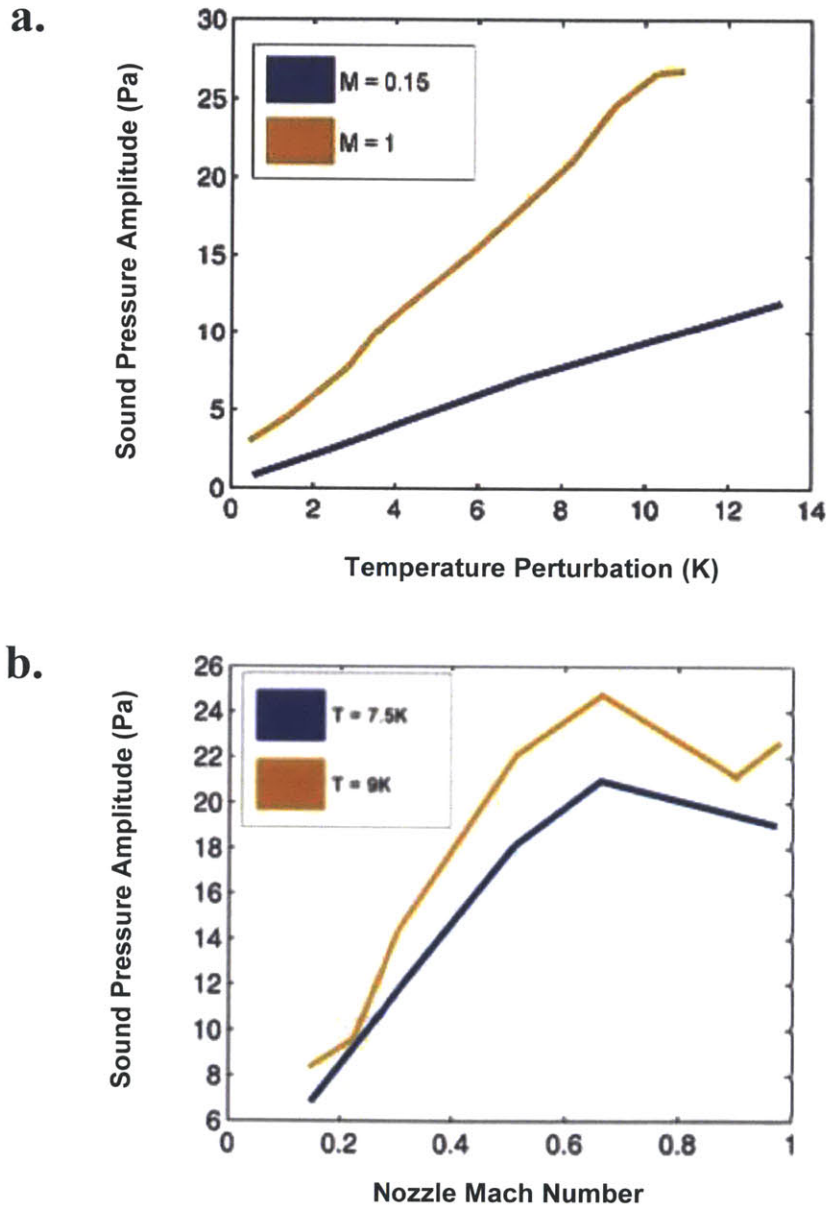


Figure 3: DLR produced entropy noise test rig data. Figure 3a shows a chart for sound pressure amplitude vs. temperature perturbation, displaying an almost linear positive correlation. Figure 3b shows sound pressure amplitude vs. nozzle Mach number, displaying a nonlinear relationship, whereby entropy noise increases with Mach number for $M < 0.7$, but decreases after $M = 0.7$.

Other laboratories have attempted to analyze entropy noise, but mostly through theoretical and numerical methods. Further experimental research needs to be conducted from an external source in order to verify DLR's experimental results and achieve greater understanding of entropy noise.

Furthermore, DLR research revealed that current theoretical knowledge of entropy noise does not match experiment trials for fluid mass flow variation. The test rig was simulated through Marble and Candel's derivations for noise generated from an isentropic system with a compact choked nozzle sustaining supersonic flow. Sound pressure waves due to entropy fluctuations were characterized by the following equation "where κ is the isentropic exponent, M_1 and M_2 the Mach numbers upstream and downstream of the nozzle or diffuser, respectively..., q'_s the impinging density fluctuation corresponding to the entropy wave ..., a_1 the speed of sound upstream of the nozzle or diffuser, and p'_{2+} the downstream propagating acoustic pressure wave" (Bake 2008).

$$p'_{2+} = \frac{M_2 - M_1}{1 + M_2} \frac{\frac{1}{2} M_1}{1 + \frac{1}{2}(\kappa - 1)M_1 M_2} a_1^2 \Delta q'_s \quad (1)$$

Their numerical methods were only able to predict actual experiment data within a nozzle Mach number range of 0.5 to 0.7. Refer to Figure 4 for an examination of numerical predictions versus experimental data, which reveals a significant difference between the two methods and a clear gap of knowledge. Discrepancies may be due to the model simplification of the nozzle as isentropic, one-dimensional, and compact. In order to find out how entropy noise functions, more research is needed.

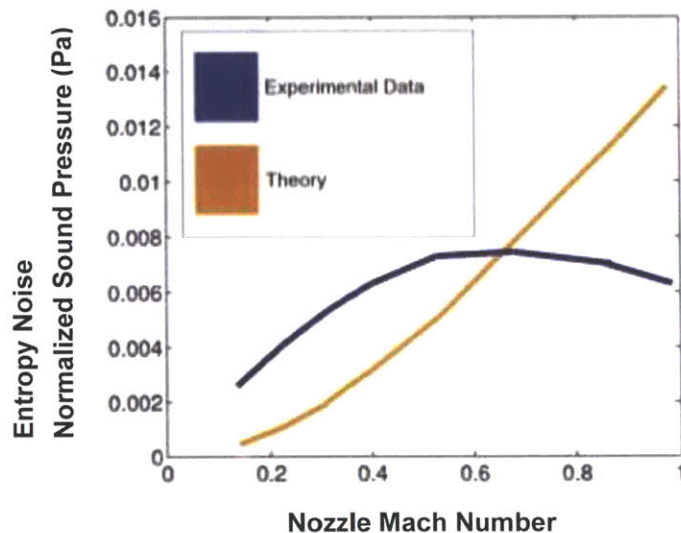


Figure 4: Orange indicates DLR's theoretical prediction from numerical analysis. Blue shows experimental data. Although there is agreement for $0.5 < M < 0.7$, the theoretical results are not in agreement with the actual data for small and large Mach numbers.

Reports about the original DLR entropy noise test rig were utilized as the starting point in Osney Lab’s endeavor to build its own experiment apparatus. Figure 5 depicts the experiment setup at DLR.

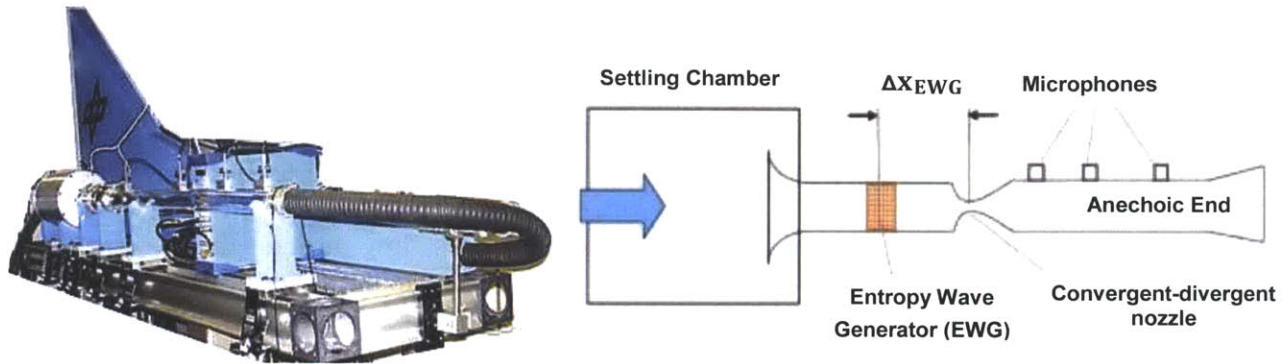


Figure 5: Pictured is a photograph and diagram of the entropy noise experiment setup at DLR. Compressed air flows into the test rig. Entropy waves are formed and accelerated through a nozzle. Microphones detect resulting entropy noise. Air exits the test rig at its termination. (<http://www.dlr.de>)

For the DLR entropy noise experiment, air injection flowed into a “heating module to generate entropy waves electrically.” Subsequently, the air accelerated through a convergent–divergent nozzle. The pressure change caused by the area change in the nozzle gave a maximum Mach number $M=1.0$. DLR used “flush-mounted microphones” along the end of the test rig to record resulting acoustic waves. The Osney lab’s project aimed to create a test rig that would show how entropy noise changes with its input variables, while keeping prior experimental design under consideration. (<http://www.dlr.de>)

2.3 Input Parameters

In the Osney Laboratory's entropy noise investigation, the main parameters of interest are upstream temperature, and nozzle Mach number. Temperature variability, representative of heat fluctuations in a combustor, is significant because entropy waves form under temperature gradients. The test rig generates entropy waves through a heating module, which creates an uneven temperature distribution in the axial direction. By adjusting magnitude and duration of the fluid's heating processes, it is possible to find the effect of aggregate temperature change on entropy noise.

The other main variable, Mach number, defines air mass flow through the test rig. Mach number, M , is given by fluid flow speed divided by the speed of sound. Therefore, Mach number less than 1 describes a subsonic test run. Similarly Mach number equal to 1 indicates sonic and greater than 1 indicates supersonic (grc.nasa.gov). A nozzle with a changing cross sectional area is employed to alter pressure and Mach number through the test rig, simulating the pressure jumps through the turbine and exhaust stages of an internal combustion engine. At DLR, Mach number in the throat of the nozzle ranged from 0.15 to 1.00 during different runs. At the Osney Lab, the Mach numbers in the nozzle should fall within a similar range, between 0.15 and 1.50.

Additional factors that can be easily manipulated with the test rig are inlet pressure, inlet velocity, distance between the entropy wave generator and nozzle, and shape of the entropy pulse (square wave versus sinusoidal). Pressure and velocity are controlled by a pressure regulator at the beginning of the rig. Distance can be altered with interchangeable pipe sections of various lengths (50mm, 100mm, and 200mm). Lastly, entropy pulse is modifiable through a circuit attached to the entropy wave generator.

3. Experimental Design

3.1 Test Rig Apparatus

The test rig is designed to simulate entropy noise in an aero engine. It makes entropy waves through electric heating and then accelerates the waves to produce entropy noise. Resulting acoustic sound is measured with microphones. The test rig allows for easy changes in temperature and Mach number. Figure 6 provides the layout of each module in the complete test rig. Compressed air enters the anechoic labyrinth through a valve. From there, it flows through the settling chamber, Entropy Wave Generator (EWG), convergent-divergent nozzle, microphone section, and finally the anechoic termination. Each module plays an important role in the experiment. Together, the full system allows for the measurement of entropy noise with varied parameters.

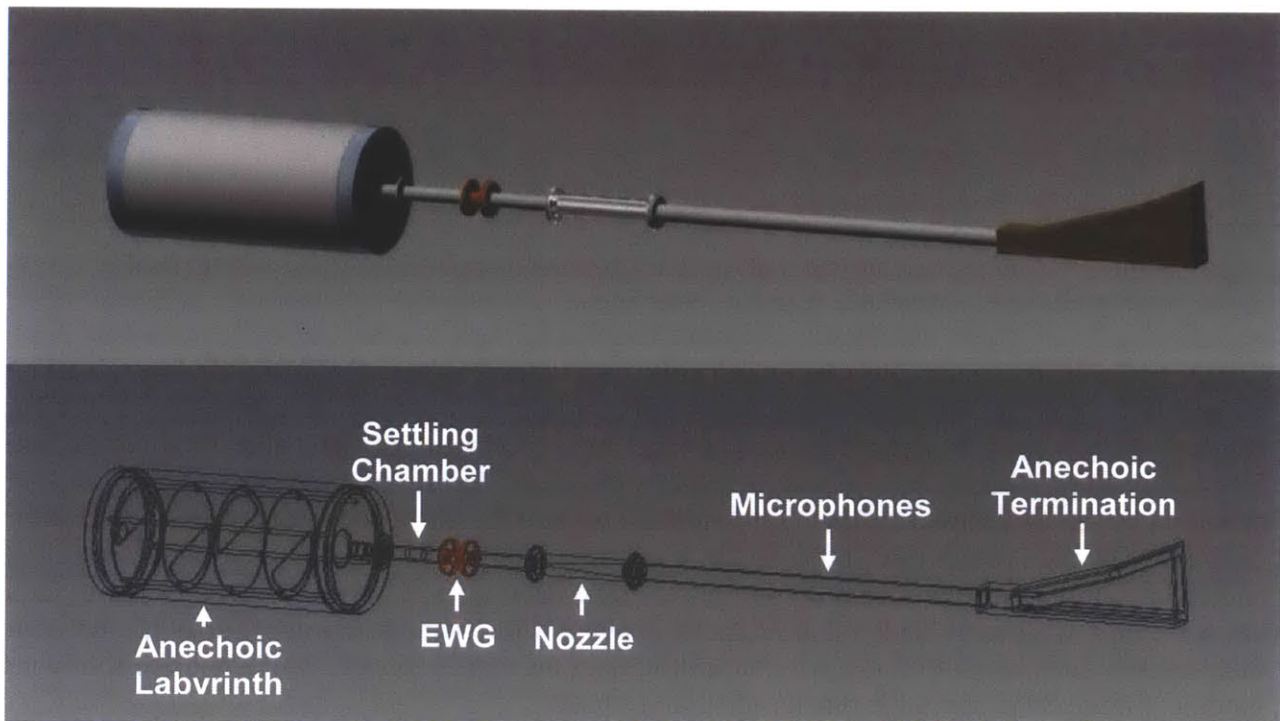


Figure 6: An entropy noise test rig models entropy noise in an aero engine. Compressed air is taken in through the anechoic labyrinth, which blocks noise from the compressed air valve. Then air enters the settling chamber, which calms air flow. The EWG creates entropy waves. Entropy waves pass through a nozzle with a convergent-divergent shape to accelerate the air and alter Mach number. Microphones are stationed along the subsequent tube to measure acoustic waves from entropy noise. An anechoic termination prevents reflections at the end. Knowledge of entropy noise compared to input variables can be ascertained through this setup.

3.2 Anechoic Labyrinth

The purpose of the anechoic labyrinth is to absorb sound produced by the compressed air source at the intake valve (see Figure 7). When fast-moving compressed air mixes with the static air in the rig, it causes turbulence, which creates noise. Microphones are stationed at the end of the test rig to measure acoustic noise created by entropy waves. The injection of compressed air releases sound is not the subject of experimentation. Therefore, if any excess sound from the intake valve reaches the microphones, it can interfere with entropy noise readings.

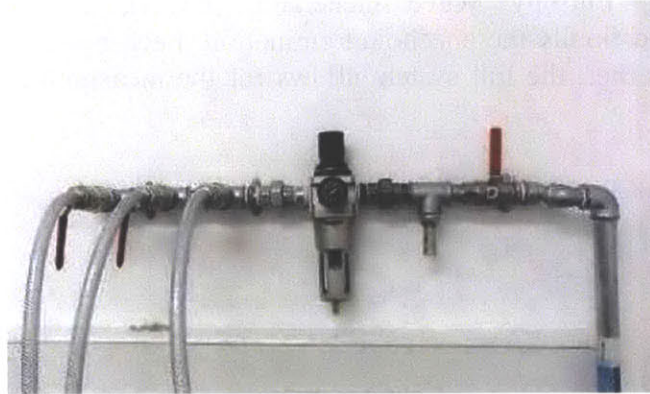


Figure 7: Compressed air is sent through a tube with an open valve to the test rig intake. Inlet pressure is controllable with the center knob.

In order to prevent faulty readings in the experiment, an anechoic labyrinth is stationed immediately after the compressed air intake valve to eliminate unwanted turbulence noise. The anechoic labyrinth is constructed within a steel tube of length 700 mm and internal diameter 304.8 mm (see Figure 8a). Inside the tube, there are laser cut stainless steel parts with semicircular cross sections. These semicircles are held in place with four rods of 12.7 mm diameter. The rods run through holes in the semicircles that are fastened in place. This semicircle and rod assembly is fitted inside the large steel tube, as shown in Figure 9. Ends of the module are sealed off with steel blanks that are held in place with Victaulic clamps. Holes are bored in the center of each blank to allow for connection with the compressed air valve and the following module. Figure 8b pictures the blanks and clamps used.

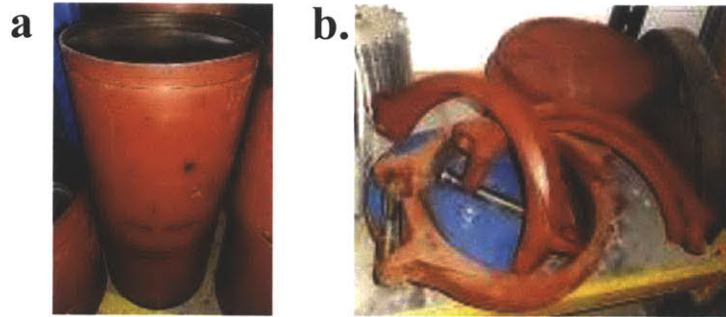


Figure 8: The test rig includes an anechoic labyrinth to block noise coming from the compressed air valve. 8a pictures the 700 mm long steel tube that houses the labyrinth. 8b shows the Victaulic blanks (upper right) and clamps (lower half) that seal off the anechoic labyrinth.

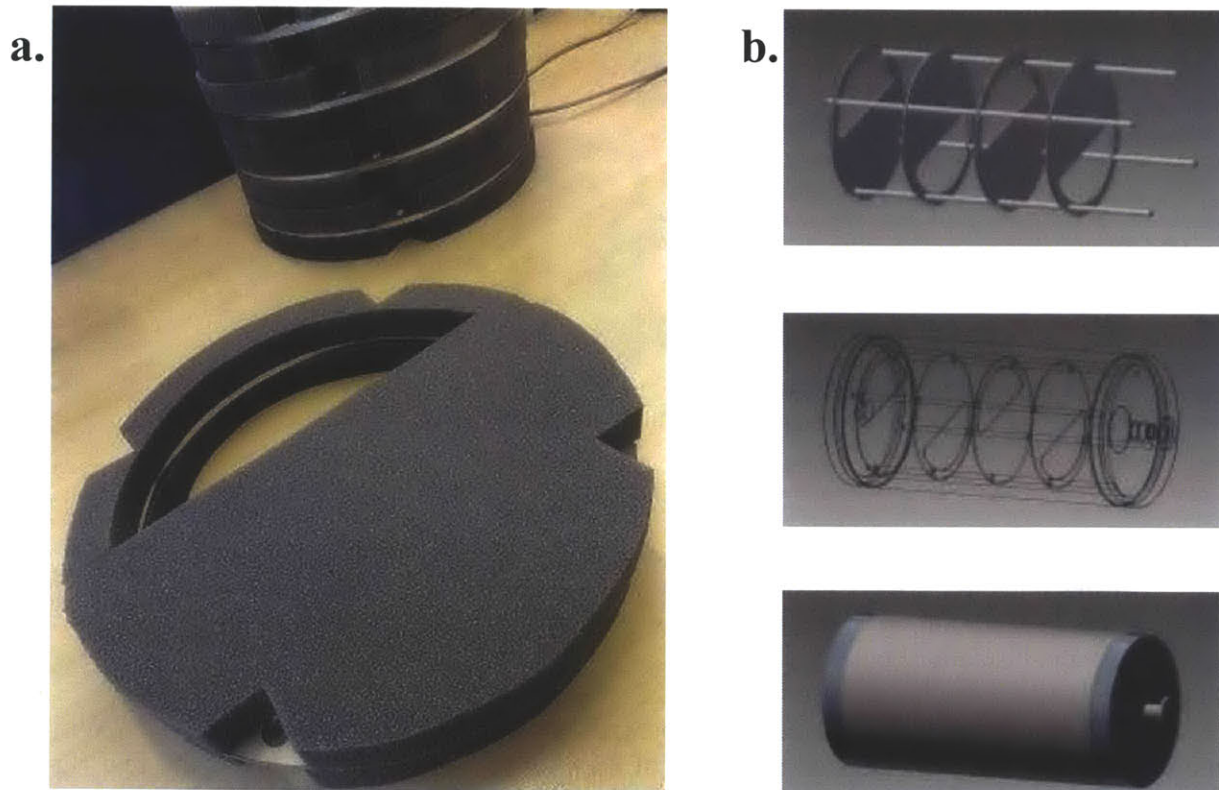


Figure 9: Stainless steel semicircular cross sections were laser cut and arranged orthogonally to the direction of airflow. By making a maze of solid parts that the air must travel through, most of the valve sound hits a semicircle, bounces off, and is reflected back toward the intake of the test rig. Sound absorbed by the foam. The semicircular sections are connected with 4 metal rods of 12.7 mm diameter. Semicircular sections are pictured in 9a. The assembly of the anechoic labyrinth is pictured in 9b with a 3D model of the final module shown at the bottom.

As air passes through the anechoic labyrinth, it hits the steel semicircle parts. These cross sections are implemented so that sound coming from upstream of the module is reflected back upstream. In other words, noise from the compressed air valve bounces back rather than continuing down through the test rig toward the microphones. A maze is constructed by installing several of these semicircles in a rotated fashion to ensure that most sound is reflected upstream. Because the pressure difference from the inlet and outlet is intended to be low for entropy noise experiments, on the order of magnitude of 0.1 bar, a series of 5 panels is a more than suitable for reducing noise to a minimal level.

Additionally, the entire surface area of the inner tube and semicircles is covered with highly absorptive foam of thickness 25 mm. This foam thickness was selected because it has sufficient absorption coefficients ranging from 0.3 to 1.0 within a broad frequency range of 250 Hz to 4000 Hz, which covers the scope of frequencies from the intake valve (kineticsnoise.com). Foam reduces sounds by lowering kinetic energy of air through molecular collisions. As air runs into the foam, sound gets trapped in the fibers of the material and turned into a trivial amount of heat. Through a combination of reflecting and absorbing sound, the acoustic labyrinth is able to minimize noise from compressed air entering through the valve before it reaches the next module. The processes of reflection and absorption are demonstrated in Figure 10.

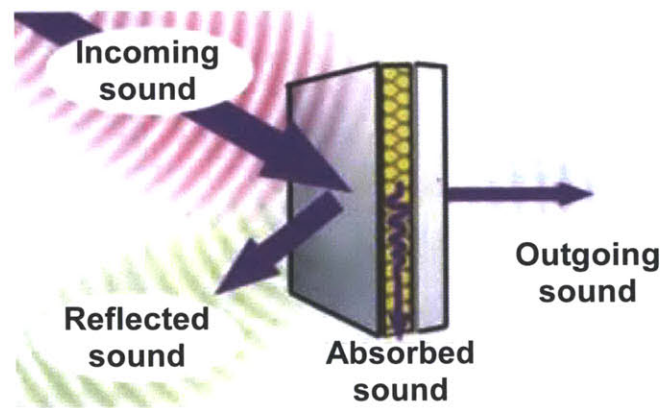


Figure 10: Some sound is absorbed by foam and most of the remaining sound is reflected off the semicircles back upstream. By incorporating several semicircle sections in the anechoic labyrinth, it ensures that very little sound actually passes through. (isover-technical-insulation.com)

Any rapid changes in area can disrupt airflow and generate unwanted noise. While the anechoic labyrinth has an internal diameter of 304.8 mm, the next segment of the test rig has a smaller diameter of only 30 mm. Hence, another important feature of the anechoic labyrinth is that air enters the next section through a bell mouth inlet. The bell mouth inlet funnels air into the rest of the system with a gradual change in area. The cross-section starts out larger, but then converges to have a diameter the size of the following pipe. In this manner, the anechoic labyrinth is able to eliminate noise from the air valve without producing noise from area change. The bell mouth taper angle is 45 degrees, which is typical as “a balance between keeping the bell mouth short without causing too much turbulence or excessive pressure drop.” (datWiki.net)

The bell mouth inlet is a solid fill 3D printed plastic part with the supporting material removed. Refer to Figure 11. It has been manufactured as two separate components so that one

side could be inserted through the hole in the exit blank before being reassembled and sealed with a solvent weld. Flanges on the end enable easy snap fit connection.

Note that, the inside sections of the blanks and the bell mouth also are coated in sound absorbing foam as an extra precaution during the area change. Air flows through the bell mouth inlet to parts downstream.

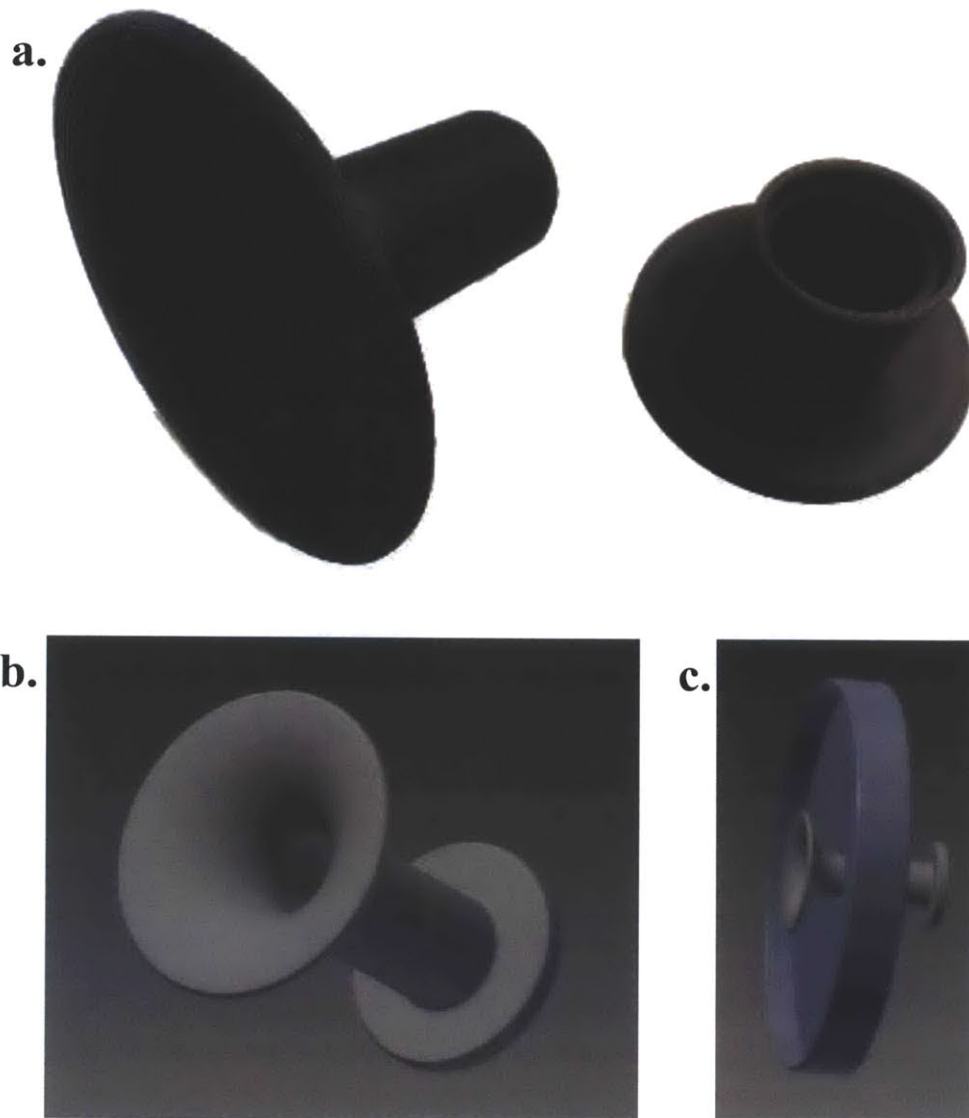


Figure 11: A bell mouth inlet is used to ease the area change from the anechoic labyrinth to the following module. 11a depicts the 3D printed bell mouth inlet components. 9b shows the AutoCad software model and 11c shows how the bell mouth inlet part should fit through a hole in the exit blank. The components are then secured together with a solvent weld.

3.3 Settling Chamber

The settling chamber is implemented to calm the airflow and reduce turbulence before entropy waves are introduced into the system. The settling chamber is comprised of an aluminium honeycomb-shape with length 500 mm and outer diameter 28 mm. A hexagonal honeycomb filter structure is “effective for removing swirl and lateral mean velocity variations” in turbulent fluid flow (Mehta 1977). Vein width is not critical for flow straightening, however the length must be at least 8 times the width to remove swirl, which is achieved in this setup. This honeycomb piece is inserted into a pipe and held in place with adhesive. As air passes through the filter, its flow straightens, converting from turbulent to laminar flow. Figure 12a depicts the honeycomb filter used and Figure 12b depicts the pipe it rests in. Once the airflow settles, it can move on to the next module.

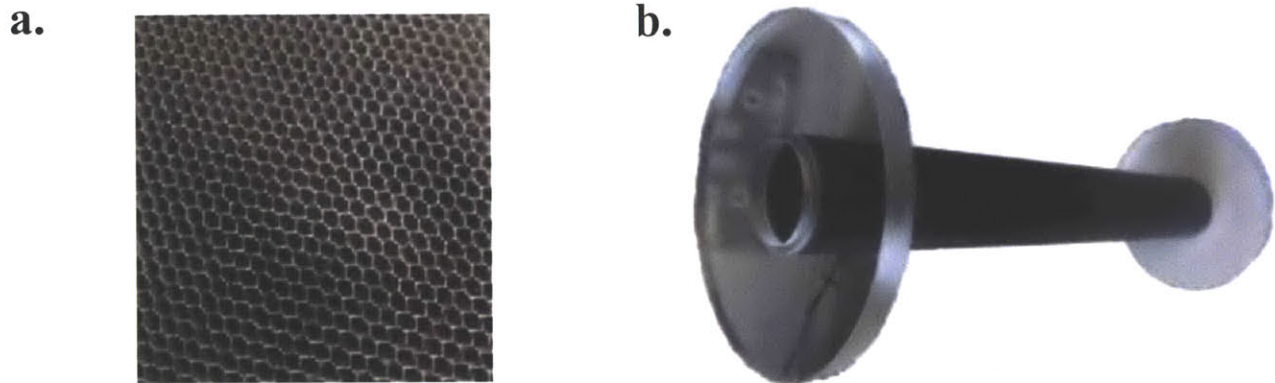


Figure 12: A settling chamber is implemented to straighten airflow. The honeycomb shaped filter, shown in 12a, is inserted into a pipe, shown in 12b.

3.4 Entropy Wave Generator

An entropy wave generator (EWG) is installed to produce entropy waves that propagate down the test rig. Entropy waves form from unsteady heat release, which produces an irregular temperature gradient. For this reason, entropy waves are introduced to the system through a heating module. The EWG raises the temperature of air via Joule heating, whereby electric energy turns into heat. Current is sent through wire and the electric energy lost due to resistance becomes heat loss. Heat then transfers to the air flowing across.

The EWG is comprised of a heat-resistant plastic tube containing 6 consecutive circular sections with metal wire stretched across. The wire is an alloy composed of 87 percent platinum and 13 percent rhodium with diameter 0.05 mm. The length of Pt/Rh wire used for each ring section is 420 mm. In each circular section, the Pt/Rh wire has been strung through holes along the surface of the tube as depicted in Figure 13 so that the wire is taut and exposed to any air passing through the system. Figure 14 displays the heating component build and drawing.

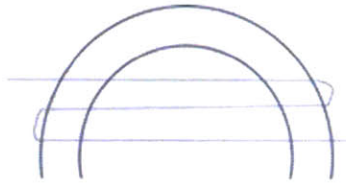


Figure 13: The entropy wave generator (EWG) heats electrically. Platinum-rhodium wires are strung through holes piercing through a housing tube like thread through a button.

a.



b.

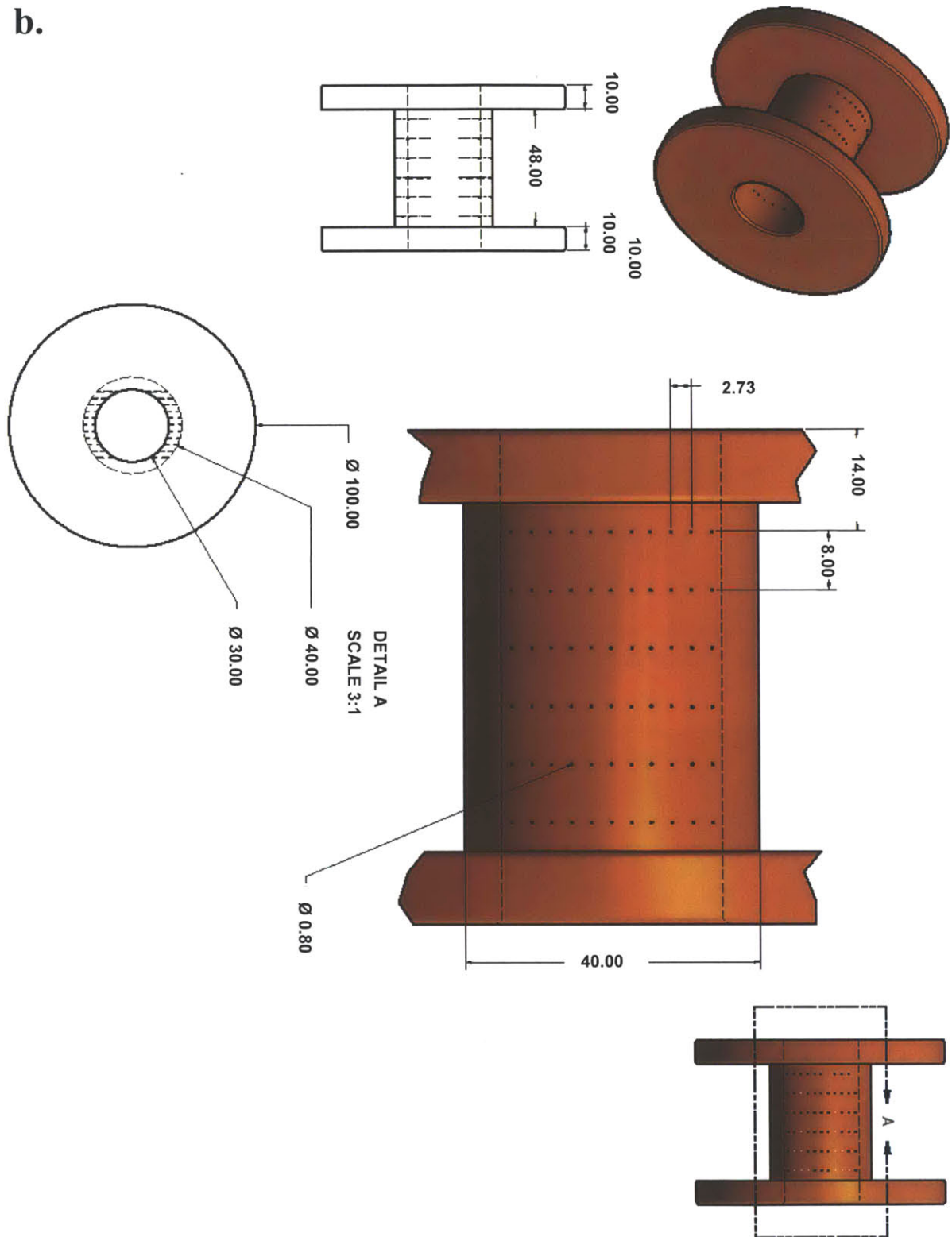


Figure 14: The heating module is pictured in 14a. Note the Pt/Rh wires stretched across the circular section with leads extending out the sides. The part drawing is depicted in 14b, showing how the part fits with the end caps. Measurements are given in millimeters.

A long copper wire has been soldered to all Pt/Rh wire ends to connect each ring section of the heating component with a power source and control circuit. The EWG control devices are displayed in Figure 15. Platinum-rhodium alloy wire has significantly higher resistance than copper wire and consequently most heat loss still occurs in the Pt/Rh wire. The attached circuit enables control of voltage and timing. By altering voltage, it is possible to get different amounts of temperature change through each ring. By running current through the ring sections at different specified times, it is possible to control which rings each section of air is heated by. Deliberate monitoring of ring delay times can produce a square wave signal or a sinusoidal signal in fluid temperature. These different manipulations of temperature signals can be implemented in experimentation to simulate various entropy distribution profiles that form in a combustor. For example, a square wave would be representative of a hot spot, but more variance in wave amplitude would be needed to model imperfect mixing.

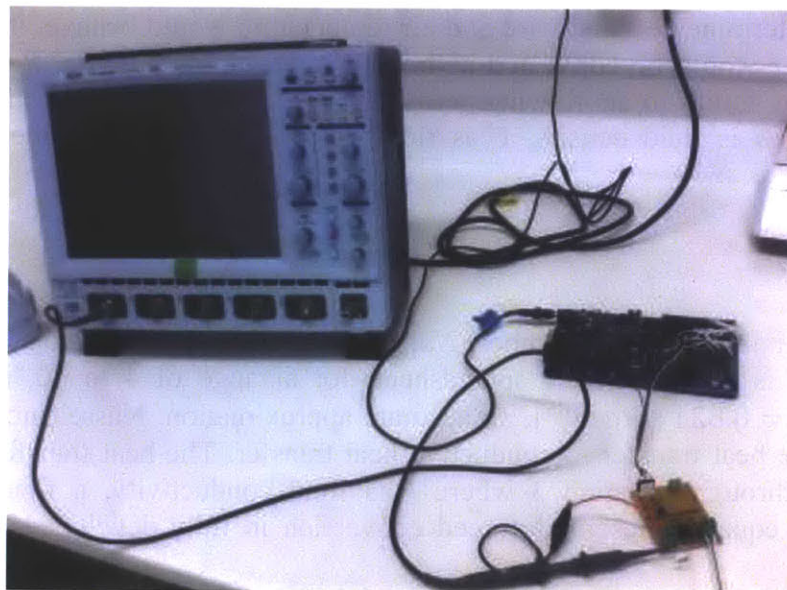


Figure 15: The heating module is connected to lab circuitry that can adjust pulse delay, duration, and intensity.

A custom spreadsheet was produced by the author to determine how wire and air temperature would change in the EWG with circuitry programming. Altering voltage is a simple way to change fluid temperature amplitude. More interestingly though, the electricity pulses phase and duration can be modified to affect the fluid temperature signal shape. Spreadsheet inputs based on parameters of the test rig set up are listed in Table 1.

Table 1: EWG Spreadsheet Input Information

Fluid (Air)			Wire (Pt/Rh)			Tube (PVC)	
density	1.1839	kg/m ³	resistivity coef	1.98* 10 ⁻⁷	Ω/ΩK	internal diameter	0.03 m
velocity	12	m/s	length	0.42	m		
viscosity	0.00002	Pa/s	diameter	0.00005	m		
specific heat	1005	J/kgK	voltage	30	V		
initial temp	293	K					

In order to determine how the wire and air temperature would behave, it was assumed that all electrical power would be convected as heat. The Reynolds number, Re , characterizes the inertial and viscous forces in air flowing across the EWG wires. Reynolds number is given by equation 2, where ρ is fluid density, U is fluid velocity, D is wire diameter, and μ is fluid viscosity.

$$Re = \frac{\rho * U * D}{\mu} \quad (2)$$

From Reynolds number, Nusselt number, Nu , is found using a correlation. For shown inputs, Reynolds number is 35.517. In the spreadsheet, for a range of 4 to 40, Nusselt number is calculated as $[Nu = 0.821 * Re^{0.385}]$, an accurate approximation. Nusselt number indicates the ratio of convective heat transfer to conductive heat transfer. The heat transfer coefficient, h , is then determined through equation 3 where k is fluid conductivity, a function of initial air temperature. This equation describes forced convection in fully developed laminar pipe flow. (sfu.ca)

$$h = \frac{Nu * k}{D} \quad (3)$$

Wire resistance, R , is calculated according to equation 4, where β is the resistivity coefficient for platinum-rhodium alloy, L is wire length per circular section, and A_c is cross section area given by wire diameter. (phet.colorado.edu)

$$R = \frac{\beta * L}{A_c} \quad (4)$$

From voltage and resistance, current, I , is found. Electric power, P_e is obtained using equation 5.

$$P_e = I^2 * R \quad (5)$$

Convective power, P_c , is defined by equation 6, Newton's Law of Cooling, (physics.info). A_s is the surface area of the wire, T_{wire} is wire temperature and $T_{in\ air}$ is the air temperature before entering the ring section. This equation is used to solve for wire temperature by equating electric power with convective power. In this step, there is an assumption that nearly all electric power

goes into convective power, which is reasonable because the bulk of electric power is contained within the EWG part.

$$P_c = h * A_s * (T_{wire} - T_{in\ air}) \quad (6)$$

Next, heat transfer is equated with convective power to find the temperature of air exiting the ring section. The calculation implemented for heat transfer, HT , is equation 7, where \dot{m} is mass flow rate (see equation 8) and c_p is the specific heat of air. (engineeringtoolbox.com)

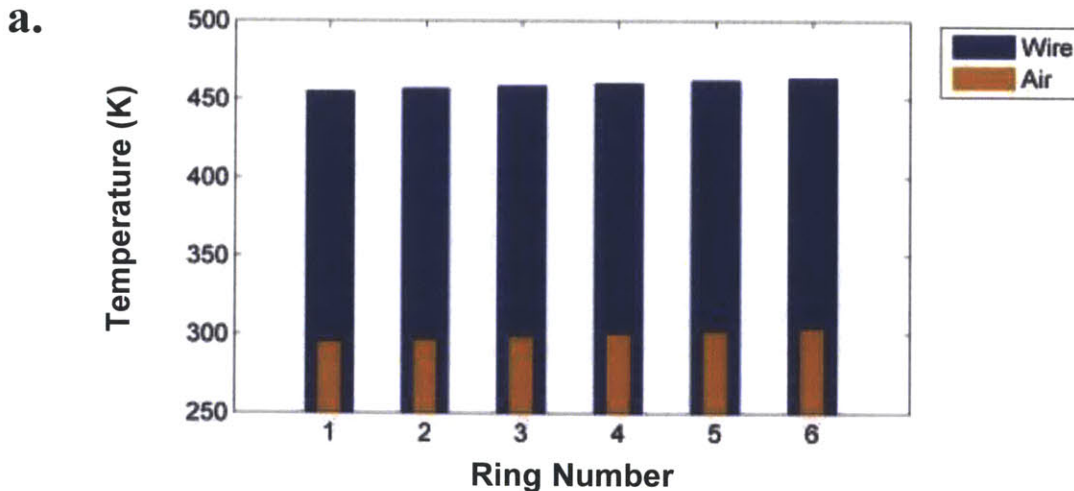
$$HT = \dot{m} * c_p * (T_{out\ air} - T_{in\ air}) \quad (7)$$

$$\dot{m} = \rho * U * A_c \quad (8)$$

Employing a combination of the above equations therefore leads to results for wire temperature at the first ring section as well as well as temperature of air once that passes through the first ring section of the EWG.

The spreadsheet calculates the wire temperature and air temperature at each stage of the EWG based on the user-inserted input information in Table 1. For ring sections 2 through 6, the value for $T_{out\ air}$ from the previous ring section becomes the new value for $T_{in\ air}$ in order to obtain values for each successive ring. If each ring section of wire is electrified as the fluid passes through, then the fluid temperature raises linearly at each ring temperature.

This analysis brings us to Figure 16a, a graph displaying the temperature change of a cross-section of air as it travels through each electrified ring. Figure 16b conveys the consistent air temperature change across each ring of approximately 2.11 K. This puts the total temperature change at 12.63 K for air that has passed through all 6 rings electrified with 30V.



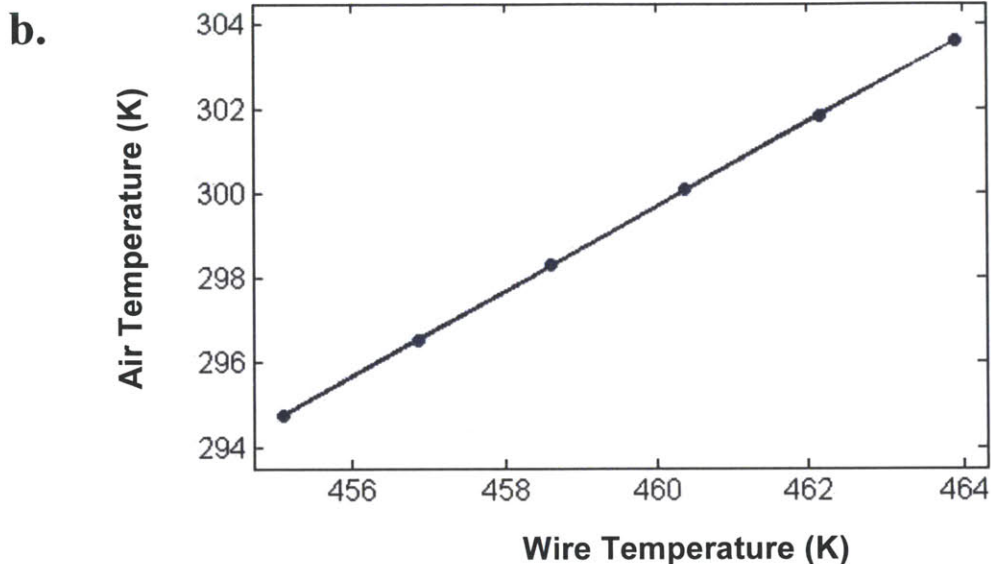


Figure 16: The graph in Figure 16a displays the wire temperature at each ring in blue. The orange bars indicate the air temperature leaving each ring. Figure 16b shows the relationship between air and wire temperature. The air temperature increases linearly as it passes through each ring section (Ring sections are indicated as dots on the graph).

Although the graphs in Figure 16 represent a cross-section of air that has passed through all 6 rings as the wires had current running through them, it is still important to consider the possibility that a cross-section of air passes through only some of the ring sections as they are electrified. The voltage sent through each ring's wire is controlled by a connected circuit (shown previously in Figure 15). The circuit is programmed to control the pulse duration and delay of current that gets sent through each wire. Accordingly, the duration of time that the current runs for in each ring is modified with delay settings. Also, the current running through each ring section can be set to start up at different times by adjusting pulse delay.

Anticipated initial testing with the rig would likely implement a square temperature wave signal. With a square wave, the amplitude of temperature change would be maximized for all sections of air that are heated through the EWG. More importantly, the resulting acoustic data would be easier to decipher with a consistent magnitude of signal coming from the EWG.

The next step in the EWG analysis was to visualize temperature change along a length of cross-sectional portions of air that passed through the EWG module. Gaining understanding for how electrical pulse duration and delay settings alter temperature profiles means that pulse duration and delay can be calibrated to establish a square wave. The spreadsheet requires additional inputs of pulse and delay for this stage. Temperature profiles reveal that the ideal pulse duration and pulse delay at an air velocity 12 m/s is 0.67 ms for both. Figure 17a shows the ideal scenario, which creates a square wave temperature change. That is, the entire section of air that passes through the EWG as voltage is sent through would be heated by all 6 rings. Figures 17b and 17c indicate setups with varied values for pulse duration and delay that causing portions of the air to reach only some of the rings when they are powered. In Figures 17b and 17c, it is

clear that those portions of the air do not reach the full temperature change of 12.63 K when the air leaves the module.

The temperature distribution that would be achieved through a square wave signal mimics a hot spot formed in the combustion chamber of an internal jet engine. The hot spot generates an uneven entropy distribution axially in the test rig pipes, which propagates downstream as entropy waves.

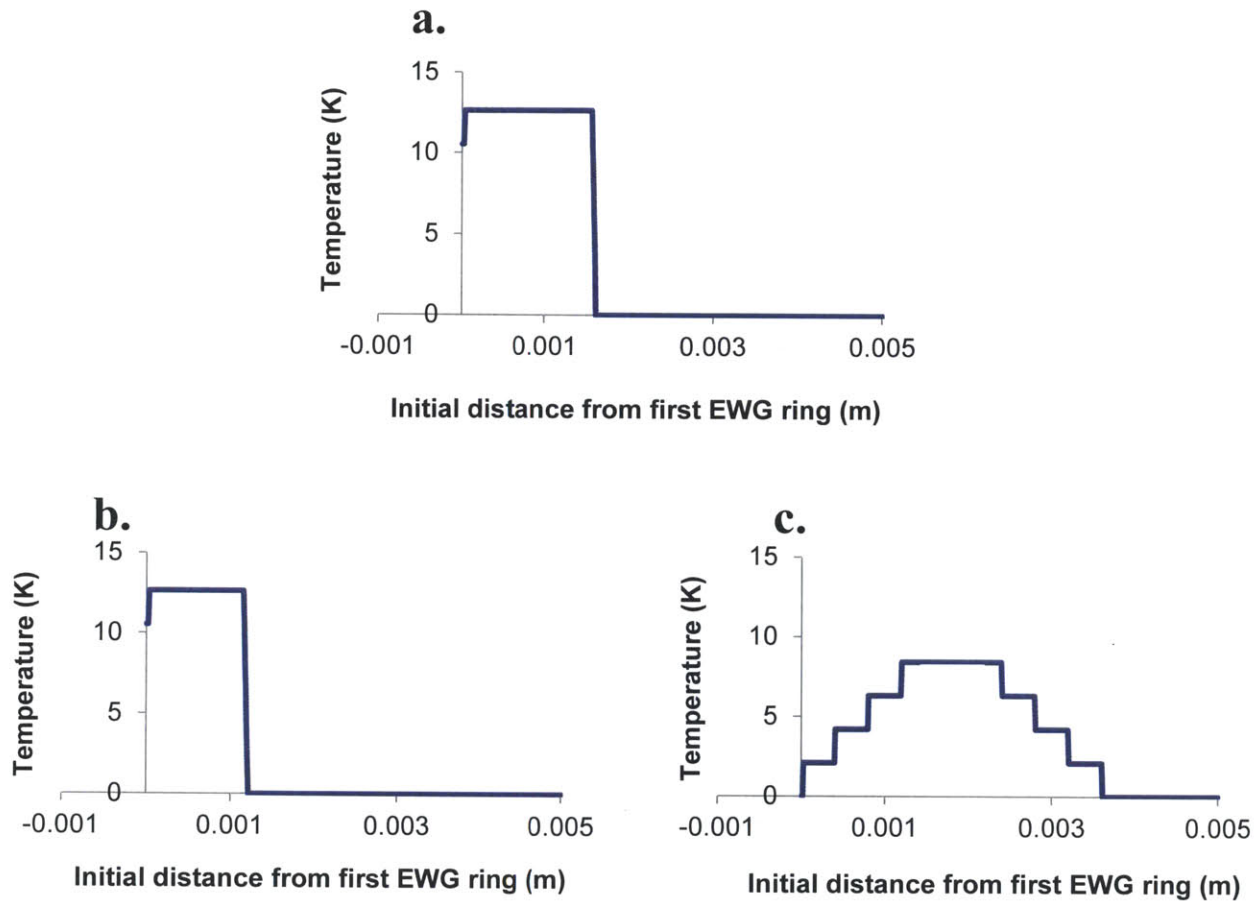


Figure 17: The graphs in Figure 17 give the temperature variation for a length of air that has passed through the EWG. They indicate total temperature change in the air once the EWG's 6th and final ring completes its pulse of current. The x axis shows the air's initial position along the test rig, with respect to distance from the start of the EWG. The y-axis shows the total temperature change for each cross section of air after it has passed through the EWG. Test rig air velocity has been set to 12 m/s, but this value is easily changeable in the spreadsheet. 17a gives the result with a duration and delay of 0.67ms. 17b gives the result if the duration is lowered to 0.5ms and the delay stays at 0.67ms. As expected, the amount of air heated is less in 17b than in 16a because the heating times are shorter. 17c gives the result if instead the duration is kept at 0.67ms and the delay is lowered to 0.5ms. As expected, different cross sections of air are heated to different temperatures because portions of the air reach some of the rings when they are not powered. Manipulating the spreadsheet predicts the temperature distribution and can therefore be implemented to create a square pulse (or a different type of pulse in the future, such as sinusoidal).

For the EWG build, it was crucial to ensure that none of the materials included would fail due to a breached melting point. Having acquired expected temperature values in the system, the material selection was re-evaluated. Although the wire temperature should not exceed its melting point of 1873 K, the tube that the wire is strung through has a much lower heat tolerance. (www.metallixrefining.com) Tufnol composite plastic is resistant up to about 473 K. The wire in contact with the outside of the tube was modeled in the worst case scenario as a flat surface flush against the Tufnol with all heat transferring to the substrate. The Tufnol was at risk of exceeding its working temperature range. Therefore, as an added measure, a vent is incorporated along the outside portion. The vent is a plastic Perspex tube (see Figure 18) with air flowing through. The air in the vent is pressurized to match the pressure inside EWG. Maintaining a consistent pressure ensures that only an insignificant amount of air escapes the heating module through external holes in the Tufnol tube.

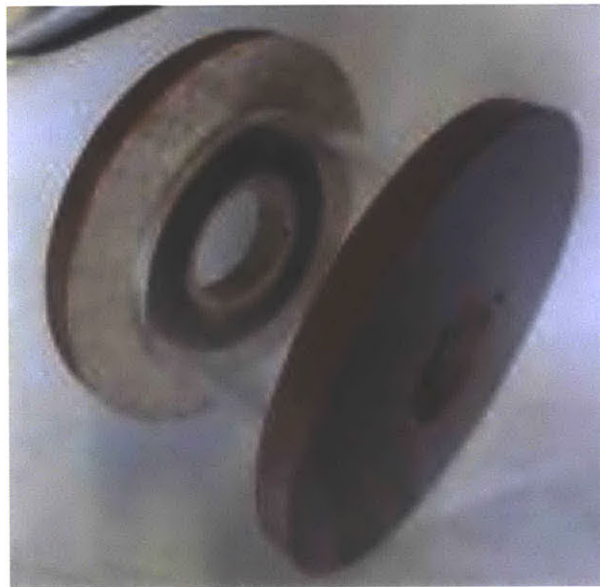


Figure 18: A vent is required so that the wire does not overheat the Tufnol tube. Air runs through a Perspex outer tube. A constant pressure is maintained so that only an insignificant amount of air escapes through the holes on the Tufnol tube.

The entropy wave generator heats the air passing through to create entropy waves that move down the system. The temperature change examined in analysis is 12.63 K. Modifications to inputs of voltage and electrical pulse duration and delay easily alters the entropy wave profile so different variations on the experiment can be performed. The square signal is of most interest now for simplicity. After exiting the EWG module, the fluid and entropy waves flow downstream through a pipe of length 200 mm. It then continues on to the next module, the nozzle.

3.5 Convergent-Divergent Nozzle

A nozzle is utilized to adjust Mach number. Its circular cross-sectional area begins with inlet diameter 30 mm, converges to throat diameter 7 mm, and then diverges to outlet diameter 40 mm. Its geometry and final build is displayed in Figures 19 and 20. The nozzle is constructed out of aluminum with conical holes that have been bored out using a milling machine.

As area is reduced toward the throat of the nozzle, pressure and air velocity increases. Mach number is the ratio of fluid speed to speed of sound. Therefore a Mach number below 1 is subsonic, equal to 1 is sonic, and above 1 is supersonic. Changing the inlet pressure or velocity produces differences in the Mach number distribution within the nozzle.

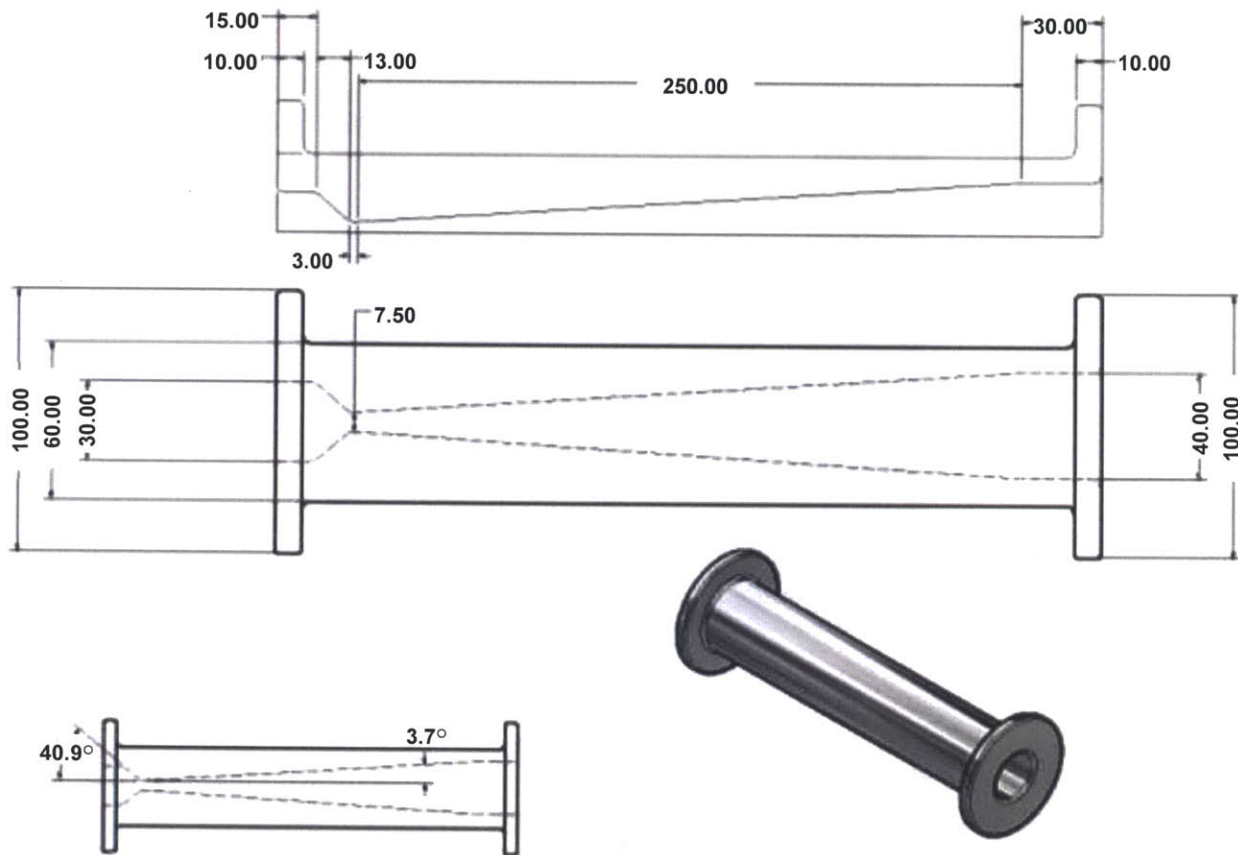


Figure 19: Figure 19 is a drawing of the convergent divergent nozzle used to change Mach number in the test rig.

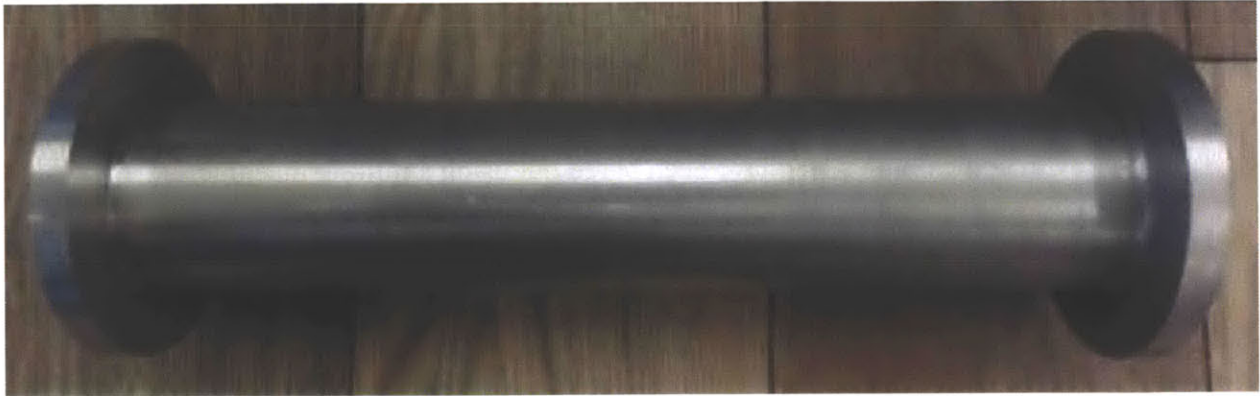


Figure 20: The aluminium nozzle is shown. The lower image displays the inlet.

Simulating the test rig nozzle geometry in Ansys Fluent software with the help of graduate student, Eduard Ron, an example Mach number distribution has been generated. This profile is featured in Figure 21. The nozzle is modeled as a pressure inlet and pressure outlet, with plenum pressure 1.17 bar and exit pressure 1.01 bar, the pressures used in previous DLR entropy noise experimentation. In this example, the Nozzle is choked soon after the throat, where the Mach number reaches its highest value of approximately 1.3.

The nozzle behaves in a predictable manner, increasing pressure with decreasing area and then decreasing pressure with increasing area. When the entropy waves go through the nozzle, they are accelerated and distorted. The behavior of the waves within the nozzle module generates entropy noise. After exiting the nozzle, entropy noise can be measured through the measurement end.

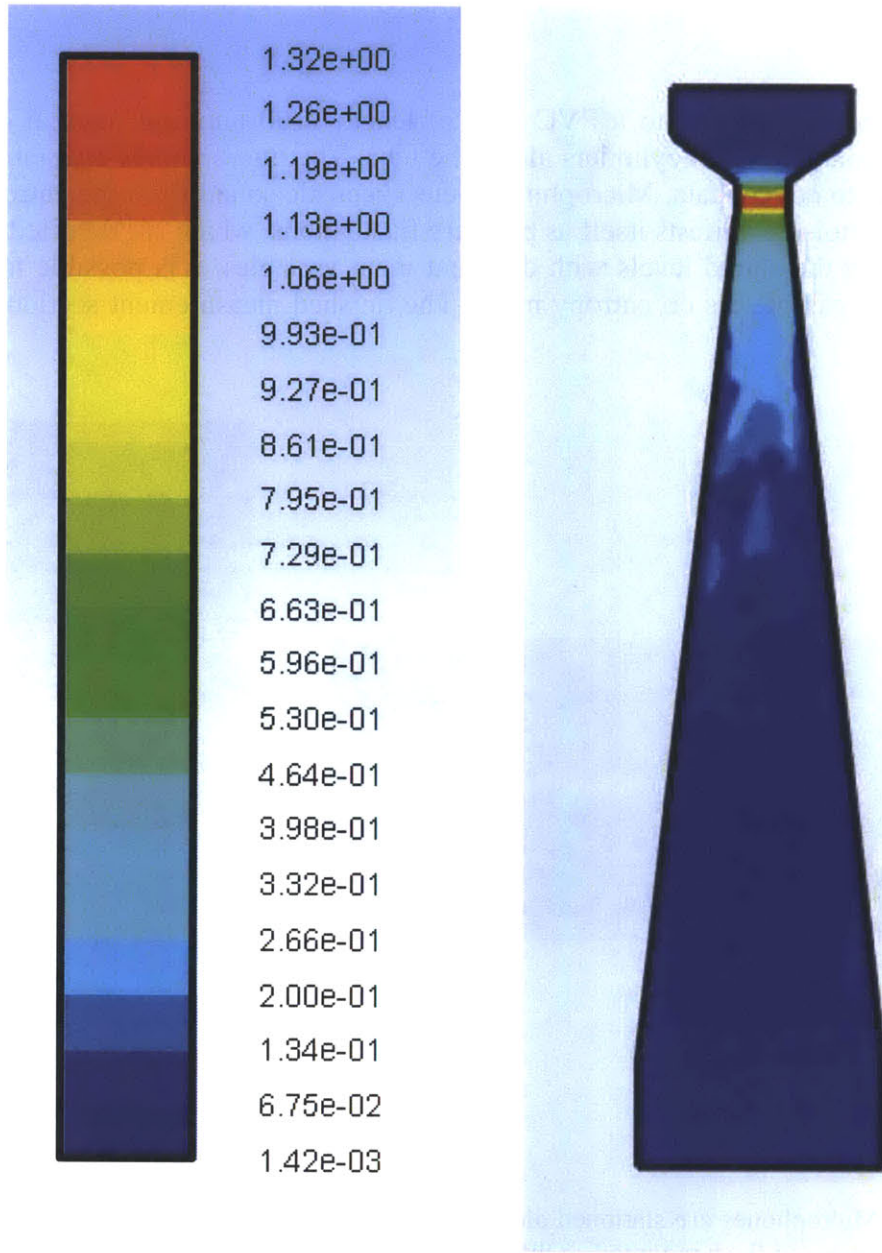


Figure 21: Computational fluid dynamics analysis through Ansys Fluent software shows a sample Mach number distribution in the nozzle. The top is the inlet and the bottom is the outlet. Mach number is at its highest right after the throat, where the fluid chokes, reaching supersonic levels.

3.6 Microphones

Four microphones are affixed to a PVC pipe of length 1160 mm and internal diameter of 40mm with flush mounted metal cylinders along the tube. The microphones are stationed along this portion in order to collect data. Microphones detect acoustic sound from the entropy noise in the system. Entropy noise manifests itself as pressure fluctuations, which are detected as acoustic sound. By measuring the sound levels with different input variables, it is possible to determine the effect of various parameters on entropy noise. The finished measurement section is pictured in Figure 22



Figure 22: Microphones are stationed along a pipe to measure entropy noise in the test rig. Microphones are flush mounted so they do not disturb airflow.

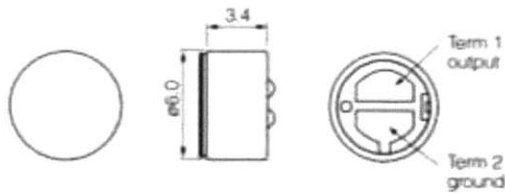
Small Panasonic omnidirectional black electret condenser microphones are used. See figure 20 for a product overview. Based on prior experimentation at DLR, the anticipated excitation sweep for sound readings is 85 to 145 Hz at 10 to 50 db. The purchased microphones cover this range and well beyond.

Specifications

Sensitivity	-35±4dB (0db = 1V/pa, 1kHz)
Impedance	Less than 2.2 kΩ
Directivity	Omnidirectional
Frequency	20-20,000 Hz
Max. operation voltage	10V
Standard operation voltage	2V
Current consumption	Max. 0.5 mA
Sensitivity reduction	Within -3 dB at 1.5V
S/N ratio	More than 62 dB

Dimensions in mm (not to scale)

WM-61A



WM-61B

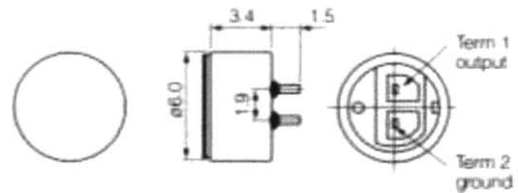


Figure 23: Microphones specifications are given in Figure 23 for product usage and to show compatibility with the expected readings from entropy noise.

3.7 Anechoic Termination

After passing through the measurement section, the air exits the test rig. It is imperative that none of the air from downstream of the measurement end produces significant noise. In order to prevent acoustic reflections from affecting the measurement portion, the termination has an approximate exponential horn shape and acoustic foam lining. An exponential horn contour is the best option for projecting low frequencies like entropy noise that fall under 300 Hz.

The exponential horn shape was modified with rectangular cross sections and straight contours to improve manufacturability. Required cross-sectional area along the length of the horn was calculated through the following equation to maintain exponential expansion:

$$A_x = A_t * e^{2z/x_0} \quad (9)$$

$$x_0 = c / (2 * \pi * F_0) \quad (10)$$

A_x is the area of the expansion at distance x from the throat, A_t is the area at the throat, and F_0 is the cutoff frequency, which for DLR experimentation was recorded as 20 Hz. (Melhuish 2008)

A graph of area change over distance for an exponential horn shape is depicted in Figure 24.

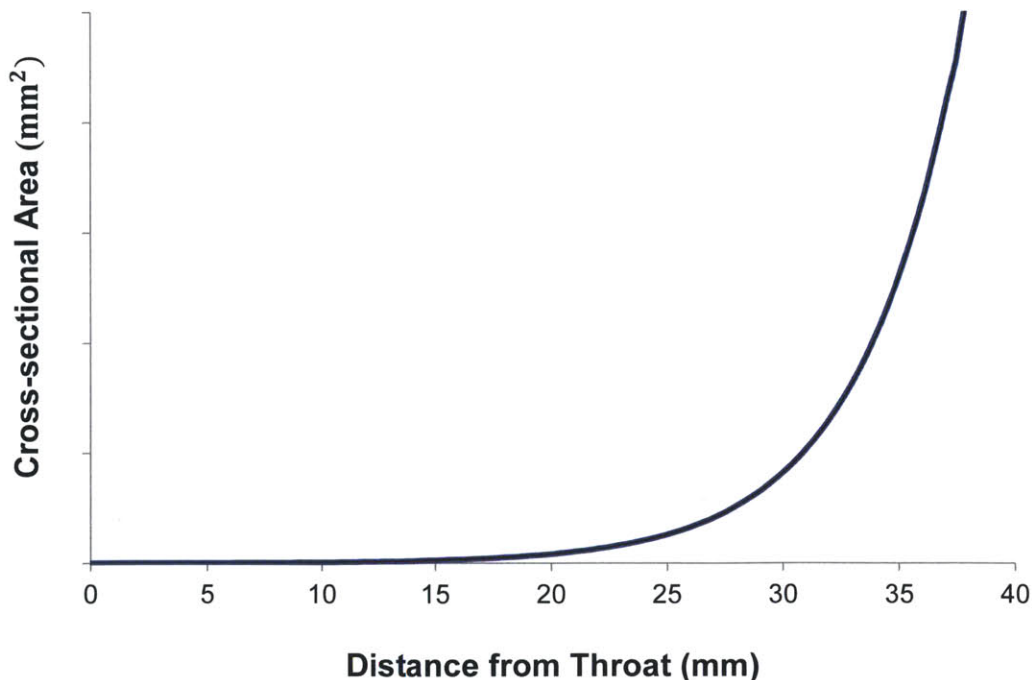


Figure 24: The area for an exponential horn expands as distance from the throat increases. Implementing a horn that maintains the shape of this function will prevent sound reflections upstream.

The expanding contour prevents reflections while foam is used to absorb sound. The termination is built from plywood assembled with screws. The foam is held in place with adhesive. See Figure 25 for a model of the module and refer to Figure 26 for a view of the constructed module. The anechoic termination completes the test rig.

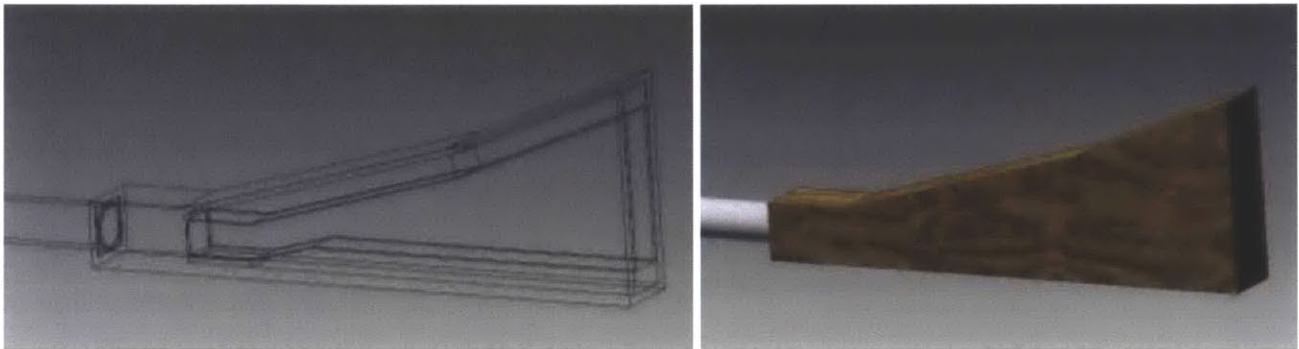
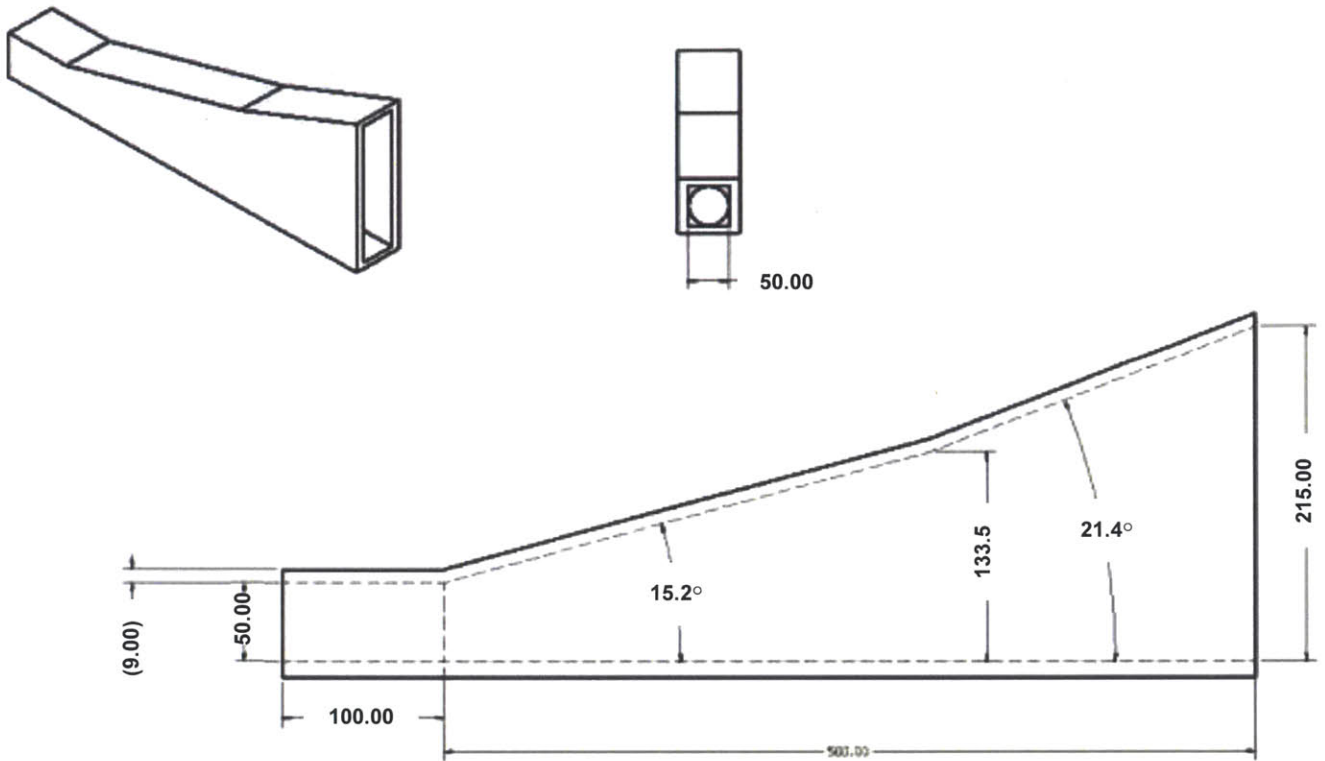


Figure 25: The anechoic termination is important for making sure sound does not travel back toward the measurement section. It has an approximate exponential horn shape and is lined in foam to project and absorb unwanted sound.

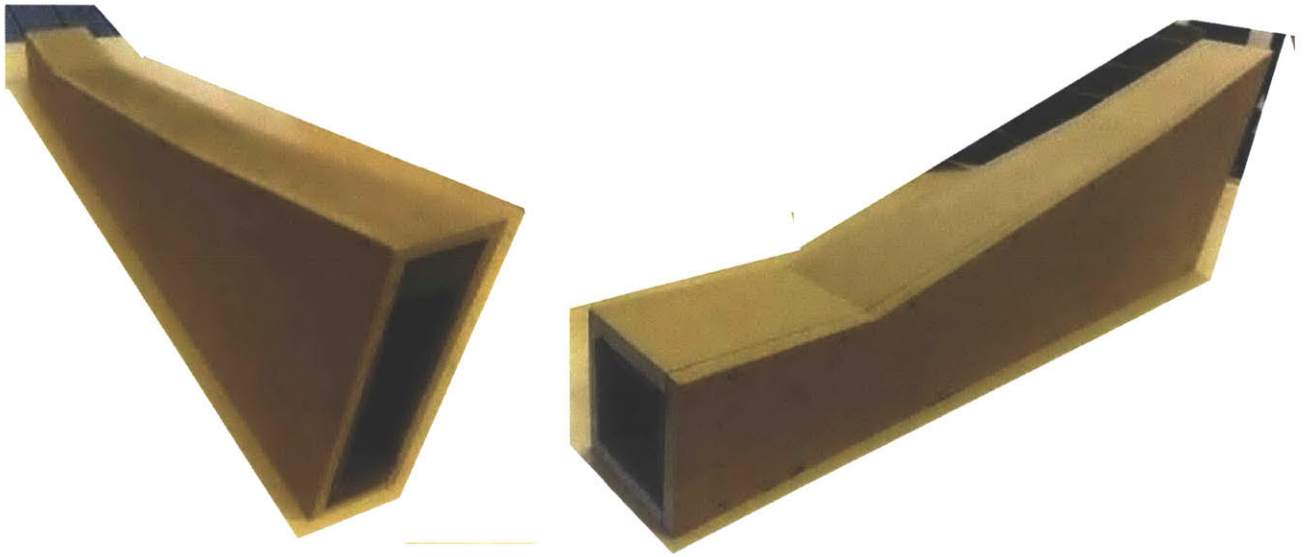


Figure 26: Figure 26 pictures the completed anechoic termination constructed out of plywood and lined in foam.

4. Method

Experiments are to be conducted by Eduard Ron, PHD student at the Osney Thermo-Fluids Laboratory using the designed test rig. First the test rig can be implemented to repeat experiments done at DLR and determine if the data is compatible. Analysis should also be done to compare experimental data with theoretical data. Beyond this stage, variations on entropy noise signals and flow parameters can be tested in order to determine the best design considerations for jet engine entropy noise reduction.

During testing, compressed air is injected into the test rig intake and sent through the system. An entropy wave signal is triggered by sending a current through the entropy wave generator. This current is controlled with the attached circuit and oscilloscope to produce a square entropy wave signal. Microphones are turned on and ready to take measurements. The microphones convey the amount of entropy noise created before air exits the test rig by picking up sound pressure waves. The entropy pressure waves are normalized to total pressure to obtain readings for entropy noise. By comparing variations in entropy noise with variations in input data like temperature change and Mach number, it is possible to figure out how entropy noise depends on its inputs.

5. Conclusion

Prior entropy noise experiment literature was compiled and reviewed. 3D CAD designs for a new entropy noise test rig were created. The design for each component in the test rig was evaluated, improved, and reassessed until deemed suitable for the project. Material specifications were chosen based on strength, heat-resistance, corrosion, purpose, and accessibility. Part manufacturers were chosen and overseen until part completion so that modules would be ready for assembly.

The Osney Lab has a test rig with the capability of measuring entropy noise. Through future experimentation, greater understanding about entropy noise can be obtained. This information is of great use to jet engine manufacturers to reduce excess sound. Future experiments will investigate the effect of temperature change and Mach number and possibly also pressure change, fluid velocity, test rig geometry, and entropy wave signal shape. If the Osney results reflect the results submitted by DLR, then their data is supported. Because current experimental data and theoretical values for entropy noise do not match, further experimentation and knowledge gain on the subject of entropy noise is important.

References

1. "Acoustical Foam Sound Absorber." *Kinetics Model KUA*. Web. <kineticsnoise.com>
2. Bake, Friedrich. "Fundamental Mechanism of Entropy Noise in Aero-Engines: Experimental Investigation." 2008. Web. <nespower.asmedigitalcollection.asme.org/>
3. Bake, Friedrich, U. Michel, I. Roehle. "Investigation of Entropy Noise in Aero-engine Combustors" Power for Land, Sea and Air. *Institute of Propulsion Technology*. 2006. GT2006-90093.
4. "Bell-mouth Inlet Duct (gas Turbine Engine Component)." *Aviation Supplies and Academics, Inc*. Web. <datwiki.net>
5. "Convection." The Physics Hyper Textbook. Web. <physics.info/convection>
6. Dolehanty, John. C. "Noise Control Spotlight: Controlling Compressed Air Noise." Web. <www.phaseto.com>
7. *Engineering Toolbox*. Web. <engineeringtoolbox.com>
8. "Forced ConvectionHeat Transfer." *Stanford*. Web. <www.sfu.ca>
9. Garcia-Rama, Ignacio D. "Research Interests." 2012. Web. <http://www.cerfacs.fr/~duran/interest.html>
10. "Introduction to Jet Engines." 2011. Web. <engg-learning.com>
11. Leyko, M., F. Nicoud, S. Moreau, and T. Poinsoth. "Numerical and Analytical Investigation of the Indirect Noise in a Nozzle." *Center for Turbulence Research*. 2008. Web. <cerfacs.fr>
12. Leyko, M. "Numerical and analytical modelling of entropy noise in a supersonic nozzle with a shock." *Journal of Sound and Vibration*. 2011. Web. <dlr.de>
13. "Mach Number." *Glenn Research Center*. Web. <grc.nasa.gov>
14. Mehta, R. D. "The Aerodynamic Design of Blower Tunnels with Wide-Angle Diffusers." *Department of Aeronautics, Imperial College*. Aerospace Sci. 1977, Vol. 18.
15. Melhuish, James. "Horn Size and Shape." *Single Driver*. 2008. Web. <fullrangedriver.com>

16. Muthukrishnan, M., W. C. Strahle, D. H. Neale. "Combustion Noise in a Gas Turbine Combustor." *ALAA Journal*. Vol 16, No. 4. Web. <arc.aiaa.org>
17. "Noise Control: Sound Theory." 2010. Web. <isover-technical-insulation.com>
18. "Noise Pollution." *EPA*. 2012. Web. <epa.gov>
19. "Platinum, Rhodium and Thermocouple Wire." Web. <metallixrefining.com>
20. "Resistance in a wire." Phet Interactive Simulations. Web. <phet.colorado.edu >
21. Schwarz, Anna and J. Janicka. "Combustion Noise." 2009. Web. <books.google.com>
22. "Take a Journey through a Jet Engine." Rolls Royce. Web. <rolls-royce.com>
23. "The Jet Engine: A Historical Introduction." *Stanford*. 2004. Web. < cs.stanford.edu >